Electronic Supplementary Material (ESI) for Catalysis Science & Technology.
This journal is © The Royal Society of Chemistry 2020

Rh Promoted In_2O_3 as Highly Active Catalyst for CO_2 Hydrogenation to Methanol

Nazmul Hasan MD Dostagir,[a,b] Coogan Thompson,[c] Hirokazu Kobayashi,[a] Ayman M. Karim,[c] Atsushi Fukuoka,*[a] Abhijit Shrotri*[a]

[a]*Institute for Catalysis, Hokkaido University, Kita 21 Nishi 10, Kita-ku, Sapporo, Hokkaido 001-0021, Japan, email:,* ashrotri@cat.hokudai.ac.jp, fukuoka@cat.hokudai.ac.jp

[b]*Graduate School of Chemical Sciences and Engineering, Hokkaido University, Kita 13 Nishi 8, Kita-ku, Sapporo, Hokkaido 060-8628, Japan*

[c]*Department of Chemical Engineering, Virginia Polytechnic Institute and State University, Blacksburg, Virginia 24060, United States*

Table of contents

Materials and methods	2-6
Figure S1-S13	7-14
Table S1-S2	15-17
Results of DFT calculations with Figure S14, S15, and table S3-S7	18-25
References	26

Materials. Indium nitrate ($In(NO_3)_3 \cdot 3H_2O$), rhodium nitrate (aqueous solution of $Rh(NO_3)_3$ (25 wt.%) and nitric acid (9 wt.%), iron nitrate ($Fe(NO_3)_3 \cdot 9H_2O$), nickel nitrate ($Ni(NO_3)_2 \cdot 6H_2O$), cobalt nitrate ($Co(NO_3)_2 \cdot 6H_2O$), ruthenium chloride ($RuCl_3 \cdot xH_2O$), hydrogen hexachloroplatinate ($H_2PtCl_6 \cdot 2H_2O$), zinc nitrate ($Zn(NO_3)_2 \cdot 6H_2O$), citric acid, sodium carbonate (Na_2CO_3) and silicon carbide (SiC) (β form, particle size 50 nm) were purchased from Fujifilm Wako Pure Chemical Corporation. Palladium nitrate ($Pd(NO_3)_3 \cdot 2H_2O$) was bought from Sigma Aldrich.

Catalyst synthesis by co-precipitation and impregnation. For catalyst synthesis using co-precipitation method, 0.1 g/mL Na_2CO_3 solution was added dropwise to a 30 mL solution of $In(NO_3)_3 \cdot 3H_2O$ (4.75 mmol) and $Rh(NO_3)_3$ (0.062 mmol) under vigorous stirring until the pH became 9. After aging for 1h under stirring condition, the precipitate was centrifuged and washed thoroughly with water. It was dried at 130 °C in an oven for 12 h followed by calcination. The catalyst was named as Rh-1.3-In_2O_3 CP.

For catalyst prepared using wet impregnation, an equivalent amount of Rh present on the surface of Rh-1.3-In_2O_3 was loaded on In_2O_3. In a typical procedure, In_2O_3 (0.5 g, prepared by sol-gel method) was dispersed in 30 mL of water followed by the addition of $Rh(NO_3)_3$ (20 μL of 0.0491 g mL^{-1} aqueous solution) and the mixture was kept under stirring at room temperature for 30 minutes. Water was evaporated under reduced pressure and then the powder was dried at 130 °C for 12 h followed by calcination. This catalyst was named as Rh/In_2O_3 WI.

Catalyst Characterization. X-ray diffraction (XRD) was measured with Rigaku MiniFlex using CuKα X-ray (λ = 1.54 Å) operating at 40 kV and 20 mA. N_2 adsorption isotherms were

measured at −196 °C using a Belsorp mini analyzer. Prior to the adsorption, all samples were degassed under vacuum at 120 °C for 2 h. Surface area was calculated by using BET theory between the relative pressure range 0.05 to 0.35 in the N_2 adsorption isotherm.[1] X-ray photoelectron spectroscopy (XPS) was performed with JEOL JPS-9010MC instrument. Charge correction was made by adjusting the external carbon peak to 284.6 eV. STEM image was obtained in a JEOL JEM-ARM200F atomic resolution electron microscope at an acceleration voltage of 200 kV equipped with EDS detector EX-24221M1G5T.

Data processing for X-ray absorption fine structure (XAFS) analysis. Data processing and analysis, for the x-ray absorption near edge and the extended x-ray absorption fine structure (XANES and EXAFS), were performed using Athena and Artemis programs of the Demter data analysis package.[2] After the normalization of the absorption coefficient, the smooth atomic background was subtracted using the AUTOBKG code in Athena to obtain $\chi(k)$ (where k is the photoelectron wave number). The theoretical EXAFS signal for Rh-O, and Rh-In scattering paths were constructed using the FEFF6 [3] code using the crystal structure of In_2O_3 and replacing the central In atom with a Rh atom.[3] The theoretical EXAFS signals were fitted to the data in r-space using Artemis. The spectra were fitted by varying the coordination number of the single scattering paths, Rh-O and Rh-In/Rh, the effective scattering lengths, the bond length disorder of each path and the correction to the threshold energy, ΔE_0 (ΔE_0 was the same since all the paths were calculated using the same model). S_0^2 (the passive electron reduction factor) was obtained by first analyzing the spectrum for a Rh foil, and the best fit value (0.85) was fixed during the fitting. The k-range used for Fourier Transform of the $\chi(k)$ was 3-13.9 $Å^{-1}$ and the r-range for fitting was 1.2-2.0 Å for fitting Rh-O scattering path only and 1.2-4.0 Å for fitting the

full model including Rh-O and Rh-Rh paths. The best parameters fit using a k-weight of 1,2,3 (simultaneously) in Artemis are reported, however, the results were similar to those using only a k-weight of 2.

Equations. CO_2 conversion, selectivity of CO and CH_3OH and space time yield (STY) of CH_3OH were calculated using the following equations.

CO_2 conversion:

$$X_{(CO_2)} = \left(\frac{nCO_{out} + nCH_3OH_{out}}{nCO_{2\,out} + nCO_{out} + nCH_3OH_{out}}\right) \times 100\%$$

CO and CH_3OH selectivity

$$S_{(CO)} = \left(\frac{nCO_{out}}{nCO_{out} + nCH_3OH_{out}}\right) \times 100\%$$

$$S_{(CH_3OH)} = \left(\frac{nCH_3OH_{out}}{nCO_{out} + nCH_3OH_{out}}\right) \times 100\ \%$$

Space time yield (STY) of methanol:

$$STY_{(CH_3OH)} = \left(\frac{SV \times [CO_2] \times X_{(CO_2)} \times S_{(CH_3OH)} \times M_{(CH_3OH)}}{22400}\right)$$

Where $nCO_{2\,out}$, nCO_{out}, nCH_3OH_{out} are moles of CO_2, CO and CH_3OH calculated from GC analysis. SV is space velocity in mL h^{-1} g^{-1}, $[CO_2]$ is the concentration of CO_2 present in the feed gas mixture in %, and $M_{(CH3OH)}$ is molecular weight of methanol in g mol^{-1}. STY of CH_3OH is reported in g_{MeOH} h^{-1} g_{cat}^{-1}.

DFT calculations. We used the Gaussian 16 rev. A.03 program and initially built a $In_{24}O_{36}$ cluster to qualitatively evaluate the chemical reactions on In_2O_3 (110) surface, where the initial geometry was the same as that of crystal In_2O_3. The DFT calculations for Rh doping on the surface were performed by using the PBE functional with the density fitting approximation.[4] Basis sets were def2-SVP for the central three metal atom sites that were potential Rh doping sites; 6-31+G(d) for O atoms surrounding the three metal atoms; 3-21+G for other O atoms; LanL2DZ for In atoms in vicinal positioning to O atoms with the 6-31+G(d) basis set; LanL2MB for other In atoms (see Fig. S14).[5] This combination was used to decrease the number of basis as much as possible so that the self-consistent field calculations converged within acceptable time (*ca.* one week using an Intel Xeon Gold 6142 processor). Suitable effective core potential (ECP) was applied for Rh and In atoms. Empirical dispersion was included by Grimme's D3 function.[6] Spin multiplicity was optimized, and the self-consistent field solution was re-optimized with the *stable=opt* option to find the most stable electronic state in all calculations. The material had three possible sites for Rh (M_1 to M_3 in Fig. S14), locating at the center of the model. After replacing one In atom with Rh, orientation of the three metal sites and surrounding O atoms was optimized, where other atoms were frozen to preserve the crystal structure. We used the *loose* level of geometry optimization [root mean square (RMS) force < 0.001667 a.u., RMS displacement < 0.006667 a.u.] to decrease calculation time. Error in electronic energy due to use of the *loose* option was less than 0.1 kJ mol^{-1}, which was accurate enough to discuss the Rh sites.

Other calculations were performed after reducing the number of atoms to 40 (Fig. S15a) at the PBE0-D3 level of theory with the *tight* level of geometry optimization (RMS force < 0.00045

a.u., RMS displacement < 0.0012 a.u.), and zero-point vibration energy was involved in the energy calculations.[7] Basis sets were slightly improved (Fig. S15a), compared to that employed for the 60-nuclei system. The In atom at the central light blue atom, corresponding to M_3 in Fig S14, was replaced with Rh when effect of doping was evaluated. To calculate the removal energy of lattice oxygen, oxygen atoms surrounding M_3 (In or Rh) were removed by the following equation: $MO_x + H_2 \rightarrow MO_{x-1} + V_{\ddot{O}} + H_2O$. For the evaluation of CO_2 activation, CO_2 was located above the left (M_2) and the central light blue metal (M_3) atoms after removing a designated number of lattice oxygen atoms around M_3. In the transition state calculations, we found only one imaginary frequency vibration and intrinsic reaction coordinates (IRC) that connect expected substrates and products.

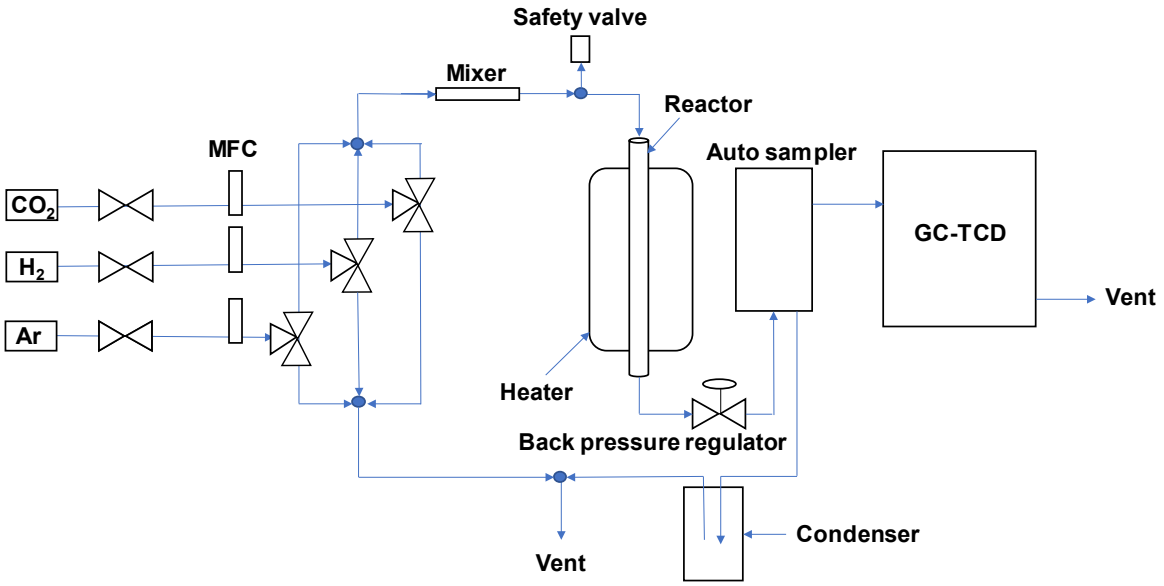

Fig. S1. Schematic representation of reaction set up.

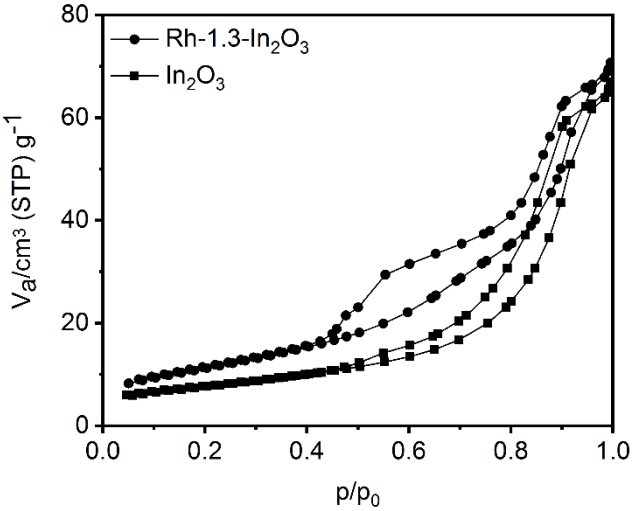

Fig. S2. N_2 adsorption isotherm of In_2O_3 and Rh-1.3-In_2O_3.

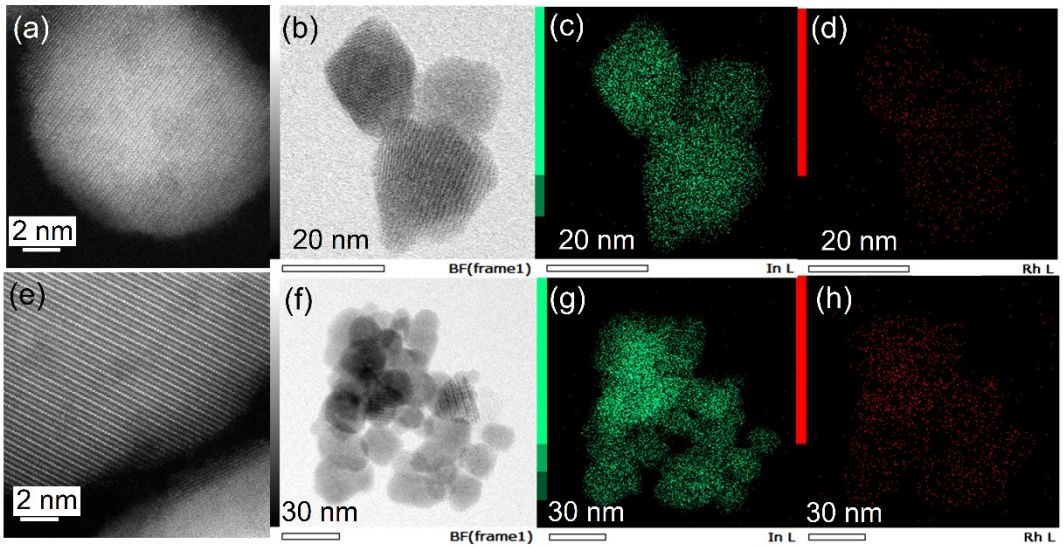

Fig. S3. HAADF-STEM images for fresh (a) and used (e) Rh-1.3-In_2O_3 catalysts. EDX mapping for fresh (b,c,d) and used (f,g,h) catalysts.

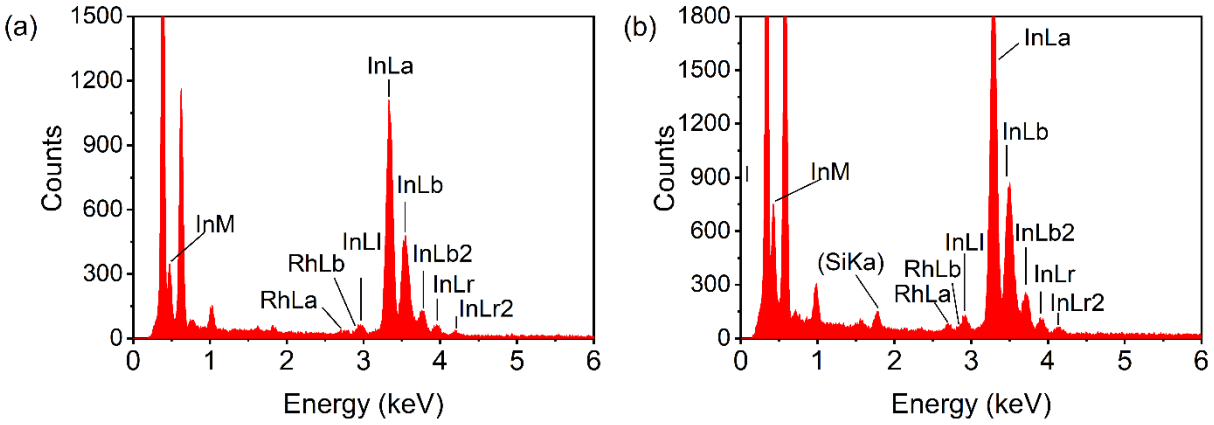

Fig S4. Corresponding EDX spectra of (a) fresh and (b) used Rh-1.3-In_2O_3 catalysts showing EDX signature peaks for Rh and In. SiKa was detected in used catalyst because of the presence of quartz wool used during the reaction.

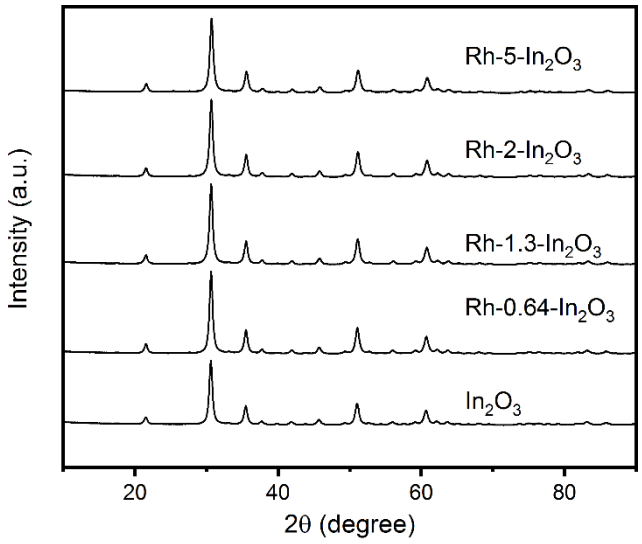

Fig. S5. XRD patterns of all catalysts. Only peaks for cubic In_2O_3 were observed at all Rh loadings.

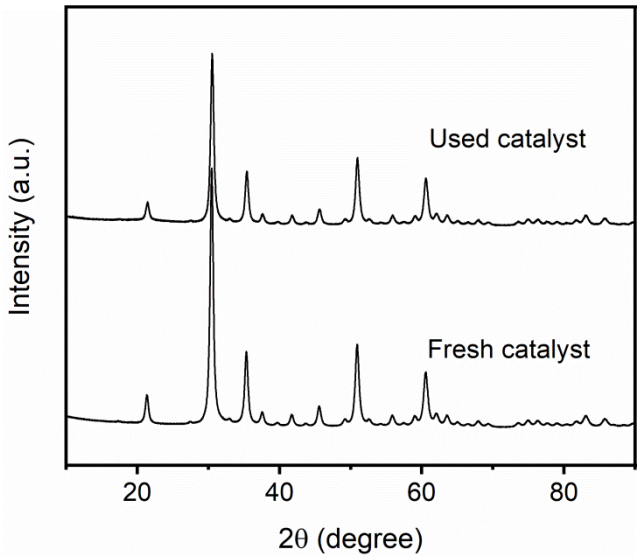

Fig. S6. XRD of fresh and used Rh-1.3-In_2O_3 catalysts.

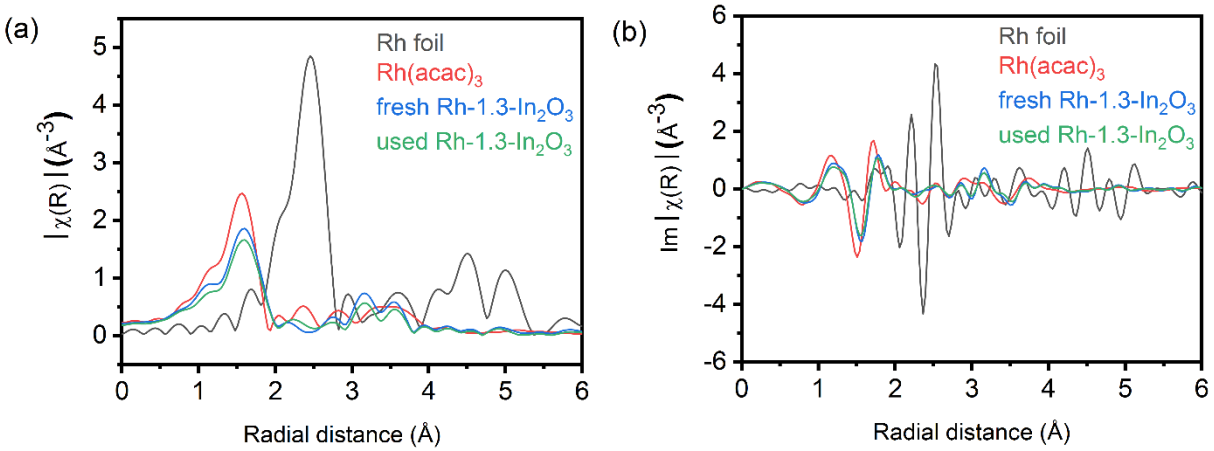

Fig. S7. (a) Magnitude and (b) imaginary part of the Fourier transformed k^2-weighted χ(k) data (Δk = 3-13 $Å^{-1}$) in R space for both the fresh and used Rh-1.3-In_2O_3 catalysts along with $Rh(acac)_3$ and Rh foil as references.

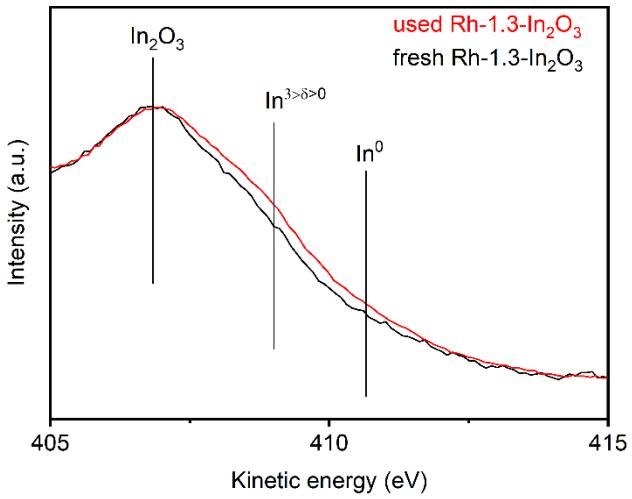

Fig. S8. In MNN peak of fresh and used Rh-1.3-In_2O_3 catalysts.

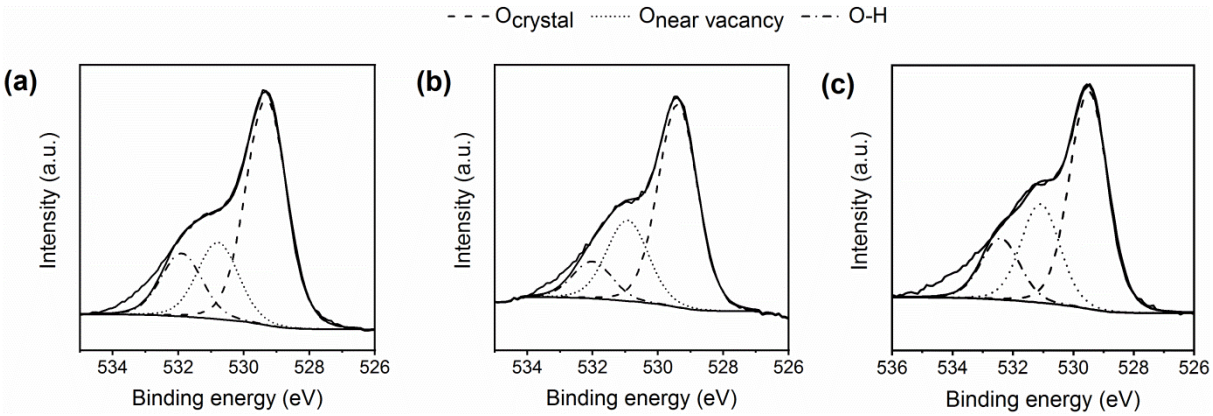

Fig. S9. O 1s XPS spectra of (a) In_2O_3, (b) fresh Rh-1.3-In_2O_3 and (c) used Rh-1.3-In_2O_3.

In_2O_3 has oxygen vacancies within its crystal structure, which gives rise to a peak at 530.9 eV in XPS corresponding to oxygen atoms adjacent to the vacancy ($O_{near\ vacancy}$). The oxygen in surface hydroxyl groups appeared as a peak at 532 eV. The cumulative of these two oxygen species is reffered as defective oxygen.

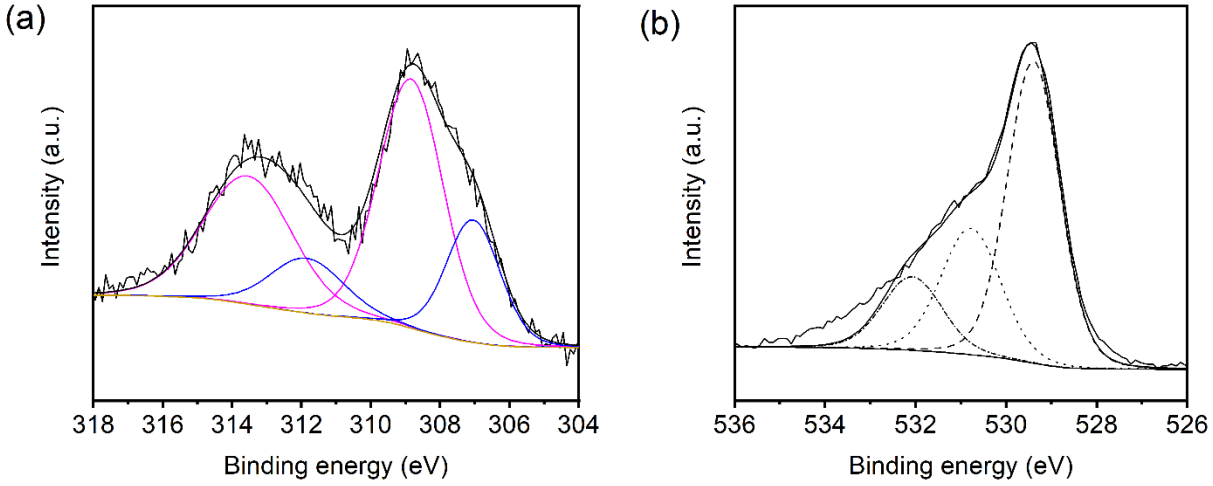

Fig. S10. XPS analysis of (a) Rh 3d and (b) O 1s after reaction for 1h. Purple and blue lines show fitting of Rh^{3+} and reduced Rh species respectively.

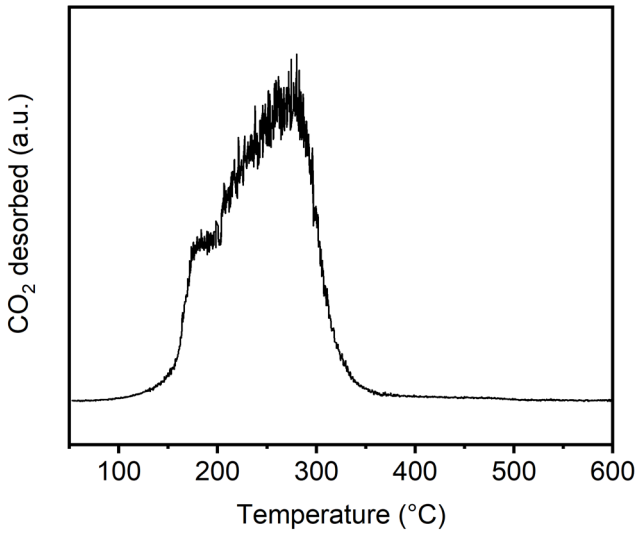

Fig. S11. Mass spectrum for evolution of CO_2 during TPD of formic acid impregnated Rh-1.3-In_2O_3 catalyst.

Figure S11 shows the evolution of CO_2 gas due to decomposition of adsorbed formic acid on the catalysts surface. The peak at 270 °C appeared at the same temperature (main manuscript, Figure 6, red line) compared to CO_2 TPD after exposing the catalyst to condition similar to reaction condition, suggesting the formation of formates species during CO_2 hydrogenation.

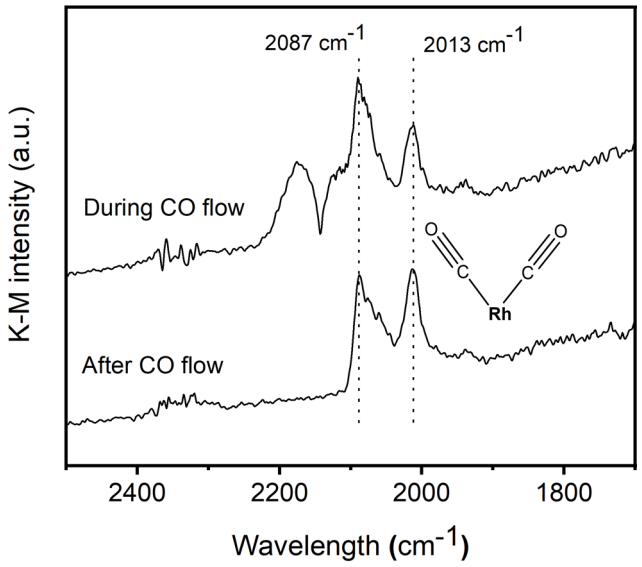

Fig. S12. CO DRIFTS over Rh-1.3-ZnO.

Adsorption of CO over Rh-1.3-ZnO catalyst shows peaks at 2087 and 2013 cm^{-1} in figure S12 which were attributed to the vibration (symmetric and asymmetric) of CO on single Rh atom, *gem*-dicarbonyl $Rh(CO)_2$. This suggests the atomic Rh dispersion in Rh-1.3-ZnO.[8]

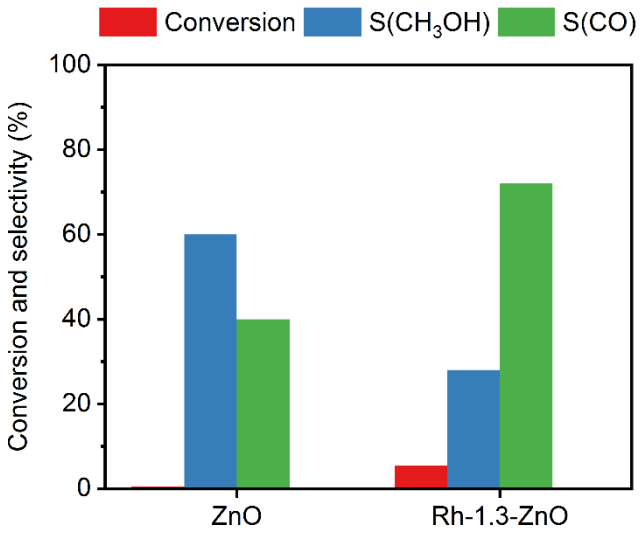

Fig. S13. Comparison of catalytic activity for CO_2 hydrogeantion between ZnO and Rh-1.3-ZnO (reaction condition: 300 °C, 5 MPa, 60,000 mL h^{-1} g_{cat}^{-1}, H_2/CO_2 = 4).

Table S1. XRD analysis of In_2O_3 and Rh-X-In_2O_3 catalysts.

Rh mol %	2Θ (degree)	d spacing (Å)	Lattice parameter (a) (Å)
0	30.57	2.921	10.1186
0.64	30.60	2.918	10.1082
1.3	30.61	2.917	10.1048
2	30.63	2.915	10.0978
5	30.66	2.912	10.0875

Table S2. Results of fitting of the EXAFS spectra for fresh and used Rh-1.3-In_2O_3 catalysts and $Rh(acac)_3$ used as reference.

Sample	Fresh[a]	After reaction[a]	$Rh(acac)_3$
N_{Rh-O}	6.1±0.7	5.2±0.6	6.4±0.9
R_{Rh-O} (Å)	2.05±0.01	2.05±0.01	1.99±0.01
$\sigma^2_{Rh-O} \times 10^3$ (Å^2)	5±1	4±1	2±2
$\Delta E_{0\ Rh-O}$ (eV)	7.0±1.3	8.3±1.2	7.9±1.9
$N_{Rh-In/Rh}$	5.3±1.8	5.3±1.8	-
$R_{Rh-In/Rh}$ (Å)	3.30±0.01	3.30±0.02	-
$\sigma^2_{Rh-In/Rh} \times 10^3$ (Å^2)	8±2	9±3	-
$\Delta E_{0\ Rh-In/Rh}$ (eV)	7.0±1.3	8.3±1.2	-
$N_{Rh-In/Rh}$	4.5±2.7	3.0±2.5	-
$R_{Rh-In/Rh}$ (Å)	3.82±0.03	3.83±0.03	-
$\sigma^2_{Rh-In/Rh} \times 10^3$ (Å^2)	8±4	7±5	-
$\Delta E_{0\ Rh-In/Rh}$ (eV)	7.0±1.3	8.3±1.2	-
Reduced χ^2	249	199	9433
R-factor	0.0086	0.0094	0.0022

[a]The coordination numbers and bond lengths for the Rh-O path in both catalysts were almost identical for the models with and without the Rh-In scattering paths. Note that the scattering from In and Rh have similar phase shift due to their similar atomic numbers. Therefore, the scattering from labelled Rh-In can also be Rh-Rh, however, the low weight loading of Rh suggests that the scattering is from In and not from Rh.

Notation: N, coordination number of absorber-backscatterer pair; R, radial absorber-backscatterer distance; σ^2, the mean square displacement of the half-path length and represents the stiffness of the bond for a single scattering path, ΔE_0, correction to the threshold energy.

Results of DFT calculations.

An $In_{24}O_{36}$ cluster model with atomic arrangement similar to 110 plane of In_2O_3, known to be the active plane for CO_2 reduction, was doped with Rh (Fig. S14). As this model contains influence of dangling bonds at the edge near reaction centers (M_1–M_3), the calculations are used for qualitative understanding of the molecular level behaviors of the material. The electronic energy evaluation suggested that Rh preferred the M_2 and M_3 sites, which were octahedral sites with five O coordination (RhO_5; Table S3). We decided to put Rh at the M_3 site as a representative promising site for Rh doping. In this case, the average Rh–O bond length (2.05 Å) in the model was found to be similar to that determined from EXAFS analysis of the catalyst, which suggested that this model is similar to the real Rh-doped In_2O_3.

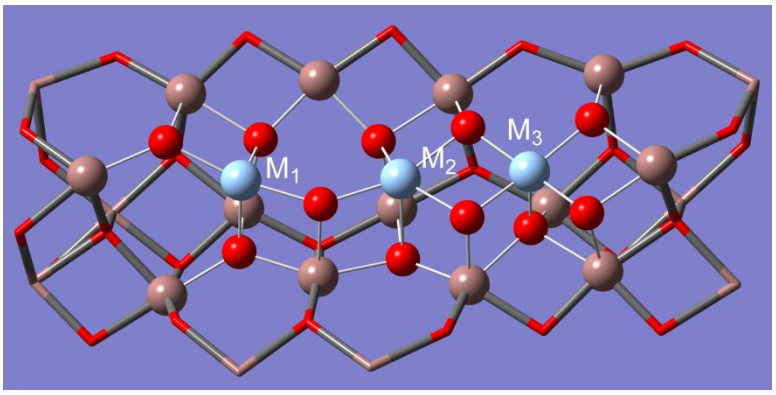

Fig. S14. $In_{24}O_{36}$ model employed in the DFT calculations for evaluating possible Rh sites. Basis sets: light blue metal atoms (M_1–M_3): def2-SVP; O atoms shown as red balls: 6-31+G(d); In atoms shown as brown balls: LanL2DZ; O atoms depicted as red stick: 3-21+G; In atoms depicted as brown stick: LanL2MB.

Table S3. DFT calculations for the Rh doping at the In sites on In_2O_3 (110) plane using a 60 nuclei model.[a]

Rh site[a]	ΔE(electronic) /kJ mol^{-1}
M_1	+33.2
M_2	+9.9
M_3	0

[a]In atoms at M_1 to M_3 sites (Fig. S14) were replaced with a Rh atom.

For the roles of Rh on the formation of oxygen vacancy, we prepared a 40-nuclei mode (Fig. S15a), a partial structure of that in Fig. S14. The M_3 site was doped with Rh as discussed above. Hydrogenation condition removed four O atoms around the Rh in a thermodynamically favored manner (RhO, $\Delta E = -110$ kJ mol^{-1}; Fig. S15b, red line), and the Rh atom was stabilized by the interaction with neighboring In atoms. In contrast, undoped In_2O_3 lost only one O atom around the In atom at the same site owing to large uphill nature of the second reduction (Fig. S15b, blue line), thus suggesting that Rh facilitates the formation of a higher density of oxygen vacancies, compared to In atoms.

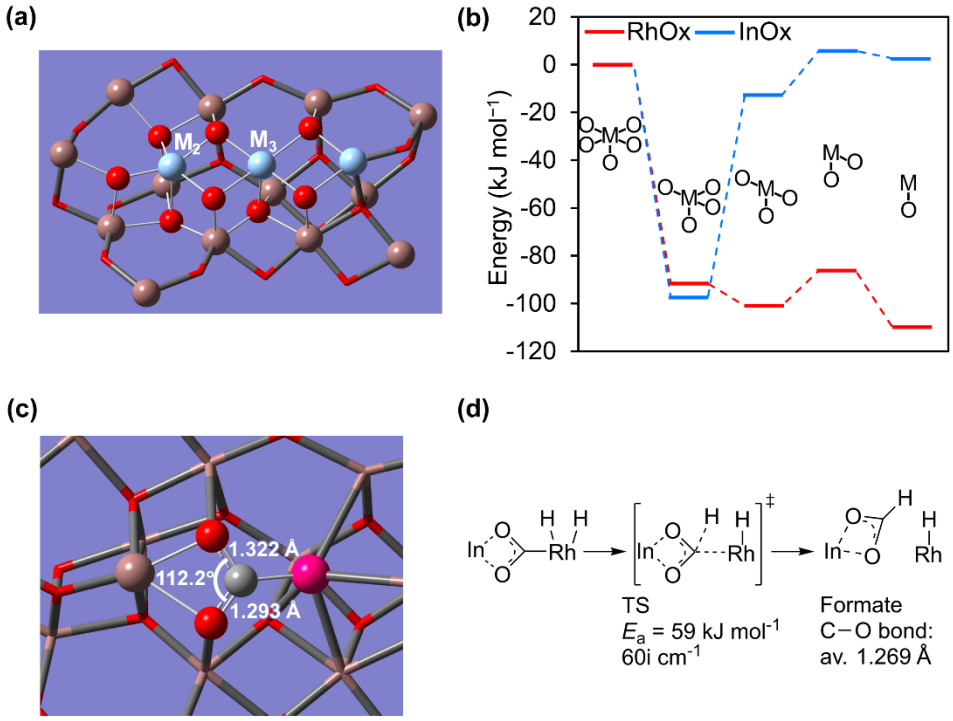

Fig. S15. Model for evaluating oxygen vacancy formation and CO_2 activation. (a) structure of this system, (b) the removal of lattice oxygen around surface Rh or In ($MO_x + H_2 \rightarrow MO_{x-1} + V_{\ddot{O}} + H_2O$), (c) CO_2 adsorption on RhO site and (d) reduction of the CO_2, where only the important centers are depicted. Gray: C; pink purple: Rh. M_2 and M_3 are corresponding to the same sites in Fig. S14. Basis sets: light blue metal atoms: def2-SVP; O atoms shown as red balls: 6-31++G(d); In atoms shown as brown balls: LanL2DZ; O atoms depicted as red stick: 3-21+G. The 6-31++G(d) basis set was applied for additional atoms (CO_2 and H_2).

We also studied the activation of CO_2 and the hydrogenation to formate, the intermediate detected in the real experiments. Introduction of a CO_2 molecule onto the RhO site produced a Rh–COO species of which the O atoms occupied two oxygen vacant sites ($\Delta E = -159$ kJ mol^{-1}; Fig. S15c). The C–O bond lengths were 0.13 and 0.16 Å longer than that of gaseous CO_2. Moreover, the COO moiety had a bending angle of 112° and a CM5 charge[9] of −0.43e, thus showing activation of CO_2.[10] Hydrogen addition to the activated CO_2 was tested after coordinating two H atoms on Rh. The H_2 dissociation to produce Rh(−H)$_2$ was energetically favorable (−54 kJ mol^{-1}). The H species smoothly attacked the activated CO_2 and successively Rh−C bond was cleaved to give formate with a low activation energy of 59 kJ mol^{-1} (Fig. S15d). The transition state appeared in the step of Rh−C bond scission rather than H transfer, thereby having a low imaginary vibration frequency (60i cm^{-1}). We also calculated a one H system, namely hydrogenation of CO_2 not by Rh(−H)$_2$ but by Rh−H. In this case, the H transfer gave a transition state with a low activation energy of 46 kJ mol^{-1}. Thus, in both cases, formate was produced by activated H species on Rh. Contrastingly, introduction of CO_2 on undoped In_2O_3 produced non-activated carbonate species (not shown). Therefore, we propose that Rh can be involved in the activation of CO_2 and the hydrogenation.

The atomic coordinates for the important structures are available as follows: Rh doping at the M_3 site (Table S4); CO_2 adsorption on Rh-doped In oxide cluster (Table S5); transition state for CO_2 hydrogenation by Rh(−H)$_2$ (Table S6); transition state for CO_2 hydrogenation by Rh−H (Table S7).

Table S4. Atomic coordinate and basis sets for Rh-doped In oxide cluster in a format of Gaussian input.

```
0 7
 In              0   -3.42265400   -0.05667000   -1.50558300
 In              0    0.63949200    0.00526900   -1.31349300
 Rh              0    3.94448100   -0.00971700   -1.40172400
 O               0   -5.29742900   -0.99376800   -1.97319600
 O               0   -3.02971800   -1.74898200   -0.22435100
 O               0   -3.63749700    1.11158900    0.30563100
 O               0   -1.39698900    0.65734600   -1.41484900
 O               0   -0.05041700   -1.74691100    0.18206000
 O               0    0.49393700    1.27426200    0.82587400
 O               0    2.38271100   -1.29314400   -1.43210300
 O               0    2.36001100    1.27530000   -1.58216900
 O               0    3.80076800    0.72026100    0.45742000
 O               0    5.57930200   -1.25739400   -1.66858000
 O               0    5.42826000    1.32980300   -1.65759800
 In             -1    0.25780700   -0.62518800    1.87010200
 In             -1    1.87926200   -2.84644600   -0.12729300
 In             -1   -3.63580600   -0.69040000    1.64335200
 In             -1   -1.63864800    1.82223600    0.46722400
 In             -1   -5.53731000    2.02079000    0.79663900
 In             -1   -1.50242700   -3.24891700   -0.41762500
 In             -1   -7.31243000   -0.16706600   -1.92436900
 In             -1   -4.90380600   -2.95028100   -0.58529200
 In             -1    5.64156000    2.02525700    0.42765900
 In             -1    4.15144800   -0.55967600    2.09632500
 In             -1    2.24001300    2.32279600    0.25967400
 In             -1    5.77750900   -3.04578900   -0.45652200
 In             -1    7.24710700    0.23940000   -2.00227100
 O              -1   -5.16802900    3.45647500   -0.78931200
 O              -1   -7.46692900    3.19078300    0.87337700
 O              -1   -1.80254300    3.62378100   -0.73355300
 O              -1    4.10472400    3.55021700    0.60139400
 O              -1    7.09332300    3.59678800    0.79521600
 O              -1    1.77090700    4.14131700   -0.95063100
 O              -1    2.26381700   -1.52581900    1.63134700
 O              -1   -1.74795800    0.27545800    2.10830700
 O              -1    0.40879900   -4.38889700   -0.79868500
 O              -1   -8.70311500   -2.15747200    1.36260000
 O              -1   -5.33302300   -2.15776100    1.38912800
 O              -1   -8.71135300    0.50144000    2.42870900
 O              -1   -8.94597800   -1.65066800   -1.57937900
 O              -1   -6.67375400   -4.18691500   -0.35927600
 O              -1   -7.00811300    0.47968600    0.12549200
 O              -1   -5.34128700    0.50123600    2.45524700
 O              -1   -3.34836700   -4.54873600   -0.46235500
 O              -1   -9.08642600    1.20873200   -1.68256100
 O              -1    5.85723700   -1.75150600    1.28434600
 O              -1    9.22728800   -1.75169900    1.31089600
 O              -1    5.84887700    0.90747400    2.35052800
 O              -1    9.18772600   -0.72736000   -1.87503800
 O              -1    7.88651500   -3.78087900   -0.43728400
 O              -1    7.55264100    0.88543500    0.04735200
 O              -1    3.70950900   -3.84019000   -0.74307700
 In             -1   -3.55545700    4.96984200   -0.81300900
 In             -1    9.02299300    2.42680000    0.71846300
 In             -1   -8.91948800    1.61970200    0.50650600
 In             -1   -7.02218800   -0.82812000    1.90891800
 In             -1    7.53795800   -0.42214700    1.83078500
 In             -1    9.65659200   -2.54455000   -0.66386400
 In             -1   -8.78284800   -3.45177200   -0.37840300
```

```
 In              -1   -0.16890400    5.10744100   -1.07853200
```

Table S4 continue

```
1-3 0
def2SVP
****
4-14 0
6-31+G(d)
****
15-27 0
LanL2DZ
****
28-52 0
3-21+G
****
53-60 0
LanL2MB
****

1-3 0
def2SVP
15-27 0
LanL2DZ
53-60 0
LanL2MB
```

Table S5. Atomic coordinate and basis sets for CO_2 adsorption on Rh-doped In oxide cluster in a format of Gaussian input.

```
0 5
 Rh              0    1.52811300   -0.22590400   -0.70777700
 In              0   -2.83281100   -0.31314100   -1.05182100
 In              0    3.98855800   -0.12681300   -1.87243200
 O               0    0.44891200    1.03149600    0.70681300
 O               0   -2.64596800    0.98081300    0.73594300
 O               0   -2.88649800   -1.99236800    0.37909900
 O               0   -4.75998300    0.16647200   -1.18440600
 In             -1   -3.87587500    4.72743900   -1.08937700
 In             -1   -2.70128500   -0.77391800    2.08867900
 In             -1   -0.98538800   -2.92723200    0.09779700
 In             -1   -4.91441000    1.40029800    0.69763000
 In             -1   -4.32035100   -3.67257700    0.04290900
 In             -1   -6.61576000   -0.79908600   -1.25740700
 In             -1    2.29309300    2.30945700    0.18229100
 In             -1    1.17269600   -0.31578400    2.06305700
 In             -1    4.50668300    0.13712300    1.57573500
 In             -1    5.62864200    3.05517200    0.23950500
 In             -1   -1.12501200    2.26622500    0.22094800
 In             -1    2.88717500   -2.76198400   -0.47048700
 In             -1    6.67684400   -1.89713600   -0.94859700
 O              -1   -5.32867100    3.11184900   -0.57196000
 O              -1    0.62464800    3.68540200    0.38430600
 O              -1    3.59927200    4.03334000    0.38465700
 O              -1   -1.84456000    3.96339000   -1.04076200
 O              -1   -0.63231300   -1.48521000    1.76542600
 O              -1   -4.76991300   -0.06133700    2.41273400
 O              -1   -2.32988000   -4.63930900   -0.40631600
 O              -1   -6.90527700    0.39453300    0.58180000
 O              -1   -5.98950700   -2.29869500    0.24271300
 O              -1    2.93854100   -1.37737900    1.20010200
 O              -1    6.28729400   -1.04690700    1.01096000
 O              -1    2.72575300    1.32113400    2.13993700
 O              -1    5.95725000   -0.19815700   -2.21002000
 O              -1    5.05681600   -3.28618000   -0.55169000
 O              -1    4.28425100    1.34192100   -0.26185800
 O              -1    0.89624100   -3.76886500   -0.58746200
 C               0   -0.19593200   -0.15444700   -1.53206300
 O               0   -0.90295000   -1.27159500   -1.52923100
 O               0   -0.94179800    0.89542900   -1.64586500

1-3 0
def2SVP
****
4-7 37-39 0
6-31+G(d)
****
8-20 0
LanL2DZ
****
21-36 0
3-21+G
****

1-3 0
def2SVP
8-20 0
LanL2DZ
```

Table S6. Atomic coordinate and basis sets for the transition state of CO_2 hydrogenation by $Rh(-H)_2$ in a format of Gaussian input.

```
0 3
 Rh              0    1.57660500   -0.50034900   -1.31014100
 In              0   -2.94023000   -0.34661100   -0.97061700
 In              0    4.01642500   -0.00869900   -1.84671000
 O               0    0.60245400    0.98793400    0.39215100
 O               0   -2.61198000    0.99184200    0.75170800
 O               0   -2.89112000   -1.98274100    0.42577400
 O               0   -4.81417100    0.23658500   -1.17485000
 In             -1   -3.86020900    4.73856000   -1.07858400
 In             -1   -2.70109800   -0.74644300    2.13397000
 In             -1   -0.98122700   -2.91235800    0.15972800
 In             -1   -4.90712700    1.42302900    0.72329400
 In             -1   -4.31700000   -3.65453200    0.09925800
 In             -1   -6.60562600   -0.78599600   -1.22378300
 In             -1    2.30235900    2.31993000    0.22491400
 In             -1    1.17368600   -0.29190000    2.11653700
 In             -1    4.50946900    0.15448700    1.63691400
 In             -1    5.63836900    3.06398000    0.28758600
 In             -1   -1.11507400    2.28094000    0.25424300
 In             -1    2.89214600   -2.75295900   -0.39716100
 In             -1    6.68504800   -1.89624100   -0.86938100
 O              -1   -5.31634400    3.12741300   -0.55641600
 O              -1    0.63458100    3.70047200    0.41396400
 O              -1    3.60954300    4.04512600    0.42097300
 O              -1   -1.82992500    3.97272800   -1.01957400
 O              -1   -0.63169000   -1.46145300    1.82045200
 O              -1   -4.76971300   -0.02963000    2.44742500
 O              -1   -2.32625900   -4.62580400   -0.33865400
 O              -1   -6.89911900    0.41820400    0.60788900
 O              -1   -5.98520000   -2.27779400    0.28642800
 O              -1    2.94122800   -1.36064800    1.26518300
 O              -1    6.29057200   -1.03459000    1.08395800
 O              -1    2.72826200    1.34354100    2.18927700
 O              -1    5.97081400   -0.20356100   -2.14269700
 O              -1    5.06224300   -3.28149700   -0.47041800
 O              -1    4.29440200    1.34870500   -0.20758700
 O              -1    0.90147700   -3.75992300   -0.51552700
 C               0   -0.60165800   -0.24298800   -2.12570100
 O               0   -1.15914800   -1.36162500   -1.80153100
 O               0   -1.24001700    0.83155600   -1.92981100
 H               0    0.38401000   -0.25200500   -2.71579300
 H               0    2.08588500   -1.44728400   -2.41878900

1-3 0
def2SVP
****
4-7 37-41 0
6-31++G(d,p)
****
8-20 0
LanL2DZ
****
21-36 0
3-21+G
****

1-3 0
def2SVP
8-20 0
LanL2DZ
```

Table S7. Atomic coordinate and basis sets for the transition state of CO_2 hydrogenation by Rh-H in a format of Gaussian input.

```
0 4
 Rh              0    1.51495000   -0.26201400   -0.97009300
 In              0   -2.91139200   -0.34992400   -1.02019900
 In              0    4.01327800   -0.11830600   -1.85720100
 O               0    0.53112300    1.04132500    0.61654500
 O               0   -2.63391700    0.98544300    0.73823700
 O               0   -2.89992100   -1.99388900    0.41277100
 O               0   -4.79934100    0.21412500   -1.19728000
 In             -1   -3.86392700    4.73405000   -1.08681300
 In             -1   -2.69748000   -0.76034800    2.10624400
 In             -1   -0.98159100   -2.92023200    0.12248400
 In             -1   -4.90725300    1.41236700    0.70754400
 In             -1   -4.31717700   -3.66267900    0.06618600
 In             -1   -6.60868500   -0.79038700   -1.24362400
 In             -1    2.30158000    2.31367000    0.19702000
 In             -1    1.17694100   -0.30580400    2.08328600
 In             -1    4.51181600    0.14284200    1.59811100
 In             -1    5.63775000    3.05649300    0.25564200
 In             -1   -1.11660000    2.27364400    0.23241700
 In             -1    2.89167800   -2.75993700   -0.44239800
 In             -1    6.68260200   -1.89974300   -0.91895000
 O              -1   -5.31870400    3.12109000   -0.56676000
 O              -1    0.63419300    3.69163700    0.39392400
 O              -1    3.60913000    4.03686900    0.39633000
 O              -1   -1.83335900    3.96827900   -1.03427200
 O              -1   -0.62884000   -1.47433400    1.78682300
 O              -1   -4.76577500   -0.04507300    2.42646500
 O              -1   -2.32714700   -4.63234900   -0.37864100
 O              -1   -6.89892100    0.40812400    0.59228500
 O              -1   -5.98527500   -2.28678000    0.26088500
 O              -1    2.94266500   -1.37117500    1.22474800
 O              -1    6.29190200   -1.04422600    1.03807500
 O              -1    2.73141400    1.32989000    2.15757400
 O              -1    5.96579800   -0.20329400   -2.18535600
 O              -1    5.06091900   -3.28631000   -0.52014300
 O              -1    4.29229000    1.34320800   -0.24272900
 O              -1    0.89994300   -3.76529900   -0.55879900
 C               0   -0.34430400   -0.26536300   -1.62533000
 O               0   -1.03472400   -1.37469700   -1.59643900
 O               0   -1.05804700    0.80181800   -1.67820800
 H               0    0.92428600   -0.25195200   -2.47014600

1-3 0
def2SVP
****
4-7 37-40 0
6-31++G(d,p)
****
8-20 0
LanL2DZ
****
21-36 0
3-21+G
****

1-3 0
def2SVP
8-20 0
LanL2DZ
```

References

1 S. Brunauer, P. H. Emmett and E. Teller, *J. Am. Chem. Soc.,* 1938, **60**, 309.

2 B. Ravel and M. Newville, *J. Synchrotron Rad.,* 2005, **12**, 537; M. Newville and *J. Synchrotron Rad.,* 2001, **8**, 96.

3 S. I. Zabinsky, J. J. Rehr, A. Ankudinov, R. C. Albers and M. J. Eller, *Phys. Rev. B,* 1995, **52**, 2995- 3009.

4 J. P. Perdew, K. Burke and M. Ernzerhof, *Phys. Rev. Lett.,* 1996, **77**, 3865; J. P. Perdew, K. Burke and M. Ernzerhof, *Phys. Rev. Lett.,* 1997, **78**, 1396; B. I. Dunlap, *J. Chem. Phys.,* 1983, **78**, 3140.

5 R. Gulde, P. Pollak and F. Weigend, *J. Chem. Theory Comput.,* 2012, **8**, 4062; R. Ditchfield, W. J. Hehre and J. A. Pople, *J. Chem. Phys.* 1971, **54**, 724; P. J. Hay and W. R. Wadt, *J. Chem. Phys.,* 1985, **82**, 270; W. R. Wadt and, P. J. Hay, *J. Chem. Phys.,* 1985, **82**, 284; P. J. Hay and W. R. Wadt, *J. Chem. Phys.,* 1985, **82**, 299.

6 S. Grimme, J.Antony, S. Ehrlich and H. Krieg, *J. Chem. Phys.* 2010, **132**, 154104.

7 J. Perdew, M. Ernzerhof and K. Burke, *J. Chem. Phys.,* 1996, **105**, 9982; C. Adamo and V. Barone, *J. Chem. Phys.,* 1999, **110**, 6158.

8 R. Lang, T. Li, D. Matsumura, S. Miao, Y. Ren, Y. T. Cui, Y. Tan, B. Qiao, L. Li, A. Wang, X. Wang and T. Zhang, *Angew. Chem. Int. Ed.,* 2016, **55**, 16054.

9 A. V. Marenich, S. V. Jerome, C. J. Cramer and D. G. Truhlar, *J. Chem. Theory Comput.,* 2012, **8,** 527.

10 X. Zhang, G. Liu, K. H. M. Broer, G. Ganteför and K. Bowen, *Angew. Chem. Int. Ed.,* 2016, **55,** 9644.